Research in Diagnostic and Interventional Imaging 8 (2023) 100035

Contents lists available at ScienceDirect

Research in Diagnostic and Interventional Imaging

journal homepage: https://www.journals.elsevier.com/redii

Original article

# Improved visualization of free-running cardiac magnetic resonance by respiratory phase using principal component analysis

Ummul Afia Shammi[a], Zhijian Luan[b], Jia Xu[c], Aws Hamid[e], Lucia Flors[d,1], Joanne Cassani[d], Talissa A. Altes[d], Robert P. Thomen[a,d], Steven R. Van Doren[b,c,*]

[a] Department of Biomedical, Biological & Chemical Engineering, University of Missouri, Columbia, MO, USA
[b] Institute for Data Science and Informatics, University of Missouri, Columbia, MO, USA
[c] Department of Biochemistry, University of Missouri, Columbia, MO, USA
[d] Department of Radiology, University of Missouri, Columbia, MO, USA
[e] Department of Radiology and Imaging Sciences, Emory University School of Medicine, Atlanta, GA, USA

ARTICLE INFO

*Article History:*
Received 9 February 2023
Accepted 15 September 2023
Available online 3 October 2023

*Keywords:*
Real-time cardiac MRI
Free-breathing MRI
Motion correction
Compressed sensing
Post-processing
Principal component analysis

ABSTRACT

*Rationale and objectives:* To support cardiac MR acquisitions during breathing without ECG, we developed software to mitigate the effects of respiratory displacement of the heart. The algorithm resolves respiratory motions and cardiac cycles from DICOM files. The new software automatically detects heartbeats from expiration and inspiration to decrease apparent respiratory motion.
*Materials and methods:* Our software uses principal component analysis to resolve respiratory motions from cardiac cycles. It groups heartbeats from expiration and inspiration to decrease apparent respiratory motion. The respiratory motion correction was evaluated on short-axis views (acquired with compressed sensing) of 11 healthy subjects and 8 cardiac patients. Two expert radiologists, blinded to the processing, assessed the dynamic images in terms of blood-myocardial contrast, endocardial interface definition, and motion artifacts.
*Results:* The smallest correlation coefficients between end-systolic frames of the original dynamic scans averaged 0.79. After segregation of cardiac cycles by respiratory phase, the mean correlation coefficients between cardiac cycles were 0.94±0.03 at end-expiration and 0.90±0.08 at end-inspiration. The improvements in correlation coefficients were significant in paired t-tests for healthy subjects and heart patients at end-expiration. Clinical assessment preferred cardiac cycles during end-expiration, which maintained or enhanced scores in 90% of healthy subjects and 83% of the heart patients. Performance remained high with arrhythmia and irregular breathing present.
*Conclusion:* Heartbeats collected from end-expiration mitigate respiratory motion and are accessible by applying the new software to DICOM files from real-time CMR. Inspiratory heartbeats are also accessible for examination of arrhythmias or abnormalities at end-inspiration.


## 1. Introduction

Cardiac magnetic resonance (CMR) is the gold standard for cardiac function evaluation with high spatial resolution and excellent soft tissue contrast [1–3]. AHA/ACC guidelines strongly recommend CMR for patients with chest pain and myopericarditis [4]. Despite the appeal of cine CMR, it requires repeated breath holds and synchronization using electrocardiogram (ECG) to guide averaging and merging of frames into a composite cardiac cycle. These can lead to blurring, prolonged exams, and discomfort for patients with arrhythmias or those unable to hold their breath due to chronic respiratory disease [5–7]. In addition, standard cine CMR does not capture the effects of the respiratory cycle upon cardiac cycles, i.e., heart rate increases with inspiration and decreases during expiration [8,9].

*Abbreviations:* BMC, Blood-myocardial contrast; CC, Pearson correlation coefficient; CMR, Cardiovascular magnetic resonance; COPD, Chronic obstructive pulmonary disease; CS, Compressed sensing; ECG, Electrocardiography; EID, Endocardial interface definition; EPI, Echoplanar imaging; BSSFP, Balanced steady-state free precession; IC, independent component; ICA, Independent component analysis; ICU, Intensive care unit; IRB, Institutional review board; MA, Motion artifact; MoCo, Motion correction; PC, Principal component; PCA, Principal component analysis; RF, Radiofrequency; RMSD, Root mean square deviation; SAX, short axis view; SD, standard deviation; TREND, Tracking Equilibrium and Nonequilibrium Shifts in Data; VD, Vertical distance

* Corresponding author.
*E-mail address:* vandorens@missouri.edu (S.R. Van Doren).
[1] Current address: Keck School of Medicine of USC, Cardiothoracic Imaging, Los Angeles, CA, USA.

https://doi.org/10.1016/j.redii.2023.100035

Real-time CMR acquisitions can cross the barriers to application of cine MRI to patients who cannot comply with breath hold instructions or who are affected by an arrhythmia that interferes in cardiac gating [10–15]. Sparse acquisitions, such as by compressed sensing (CS), matched key ventricular function results from standard cine acquisitions [15–18]. Imaging of cardiac arrhythmias and abnormal wall motion was demonstrated with real-time CMR without breath holds [14,15,19–21]. Real-time CMR is desirable to expedite imaging of children with congenital heart disease with less need to sedate them [22–24]. However, the presence of breathing motion in real-time scans presents a challenge for the interpreting physician.

Parallel imaging [25–27] and sparse sampling by compressed sensing (CS), radial, and spiral acquisitions [10,28–34] have enabled quick scanning of multiple tomographic views without need of hardware for cardiac gating or respiratory navigation [10]. Real-time MRI acquisition of many frames throughout the range of respiratory motion introduces more variability among frames, posing challenges for motion correction. Nonrigid image registration has long been used to correct respiratory motion by deforming the contents of frames to match the target frame [35,36]. Typical accuracy of registration of CMR images is 1 to 3 mm, and is challenged by respiratory motion [37]. The challenging correction of respiratory motion in $T_1$ mapping was achieved by nonrigid registration to synthetic images [38]. Nonrigid registration enhances free-breathing acquisitions by CS to be favorably competitive with cine CMR, especially in cases of arrhythmia or dyspnea [15,18]. However, the warping of the image differs between algorithms for nonrigid registration [39]. Correction of respiratory motion and artefacts has also been incorporated in reconstruction of sparse acquisitions with golden angle radial sampling using nonrigid motion fields [28] or deep learning [13] or with spiral sampling and deep learning [34].

The work herein addresses the complication of free breathing during real-time CMR acquisitions using an alternative strategy. Our objective was to accommodate the breathing of the subject. We developed software for decreasing apparent respiratory motions in dynamic CMR, by grouping heartbeats according to respiratory phase. Fundamental to our strategy is to monitor the breathing motion retrospectively using post-processing, and then segregate the cardiac cycles collected during end-expiration and end-inspiration. We evaluated the outcome of this segregation by image metrics and scoring by expert readers blinded to the post-processing.

## 2. Methods

### 2.1. Study subjects

Written informed consent was obtained from all subjects. Nineteen subjects (thirteen male, six female), aged from 24 to 73 years underwent free breathing cardiac MRI. Eight of the subjects had previous cardiac history, while eleven were healthy controls (Table 1).

**Table 1**
Demographic description of all subjects.

| Subject | Age | Gender | Height [m] | Weight [kg] | Indication | Cardiac condition |
|---|---|---|---|---|---|---|
| 1 | 24 | Female | 1.55 | 49.9 | Healthy | N/A |
| 2 | 26 | Male | 1.73 | 63.9 | Healthy | N/A |
| 3 | 26 | Male | 1.7 | 79.4 | Healthy | N/A |
| 4 | 47 | Female | 1.73 | 83.9 | Healthy | N/A |
| 5 | 63 | Male | 1.98 | 113.4 | Healthy | N/A |
| 6 | 63 | Female | 1.64 | 56.7 | Healthy | N/A |
| 7 | 65 | Male | 1.78 | 74.8 | Healthy | N/A |
| 8 | 57 | Female | 1.61 | 90.7 | Healthy | N/A |
| 9 | 59 | Female | 1.7 | 56.7 | Healthy | N/A |
| 10 | 47 | Male | 1.8 | 99.8 | Healthy | N/A |
| 11 | 72 | Male | 1.83 | 83.9 | Healthy | N/A |
| 12 | 64 | Female | 1.6 | 70.3 | Cardiac | Enlarged ventricle |
| 13 | 63 | Male | 1.88 | 95.2 | Cardiac | 1st degree AV block |
| 14 | 67 | Male | 1.8 | 97.1 | Cardiac | Coronary occlusion |
| 15 | 64 | Male | 1.75 | 95.2 | Cardiac | Diastolic heart failure; paroxysmal AFIB |
| 16 | 73 | Male | 1.8 | 79.4 | Cardiac | AFIB |
| 17 | 59 | Male | 1.83 | 108.8 | Cardiac | AFIB |
| 18 | 56 | Male | 1.83 | 106.6 | Cardiac | Paroxysmal AFIB; 1st degree AV block |
| 19 | 65 | Male | 1.79 | 125.6 | Cardiac | AFIB |

### 2.2. Imaging

The study was approved by Institutional Review Board (#2,007,146) and all subjects gave written consent. We acquired real-time CMR scans during breathing without any gating, image-based navigators, or breath-holding maneuvers. The images were collected on a 3T Siemens Magnetom Vida (Erlangen, Germany) using a BSSFP sequence [40,41], an 18-channel chest radiofrequency coil with spine coil, and CS (syngo MRXA20) to maximize spatial and temporal resolution. The acquisition rate varied from 10 to 22 frames/*sec*. Siemens software decreased the rate in cases of increased field of view. Imaging parameters were, matrix= 208 × 170, isotropic voxel dimension= 1.4 - 1.73 mm, slice thickness= 6 mm, flip angle= 30–42°, TR= 43–96 ms, acquisition time= 22–35 s. No averaging was used.

### 2.3. Algorithm to improve visualization of real-time MRI

Our algorithm groups heartbeats from real-time free-breathing MRI by respiratory phase. It exploits the ability of principal component analysis (PCA) to distinguish the respiratory motions from cycling between systole and diastole, temporally and spatially, in series of CMR images (not in k-space) [42]. The algorithm employs and automates three major steps (Fig. 1):

1 Preprocess to resolve principal components (PCs) and their time courses with potential to report on respiratory or cardiac motions.
2 Identify cardiac cycles during breaths out and in.
3 Create DICOM files with cardiac cycles at end-expiration or end-inspiration.

The preprocessing strategy was detailed previously [42]. An automatic method of extracting cardiac cycles from free-breathing, real-time CMR acquisitions at end-expiration and end-inspiration is reported herein.

#### 2.3.1. Preprocessing: implementation of PCA using trend software

Preprocessing by PCA supplied the largest time-dependent signals present in CMR scans for further scrutiny. A new software platform called TRENDimage (v. 1.9.7.1), developed from TREND [42], extracts major time dependent signal from CMR scans and transforms 3D scans into 2D data matrix while retaining the time dimension (Fig. 1). This matrix (X') is mean-centered and subjected to singular value decomposition, yielding three matrices [42] (Fig. 1):

$$X'_{mn} = U_{mn}\, S_{nn}\, V^{T}_{nn} \quad (1)$$

Here, $m$ refers to the number of rows and n to the points per row. $U_{mn}$ and $V^{T}_{nn}$ matrices are orthogonal matrices and $S_{nn}$ is a diagonal matrix. $V_{nn}$ contains the trends of change in motion over time, representing the principal components (PC) of the image series.

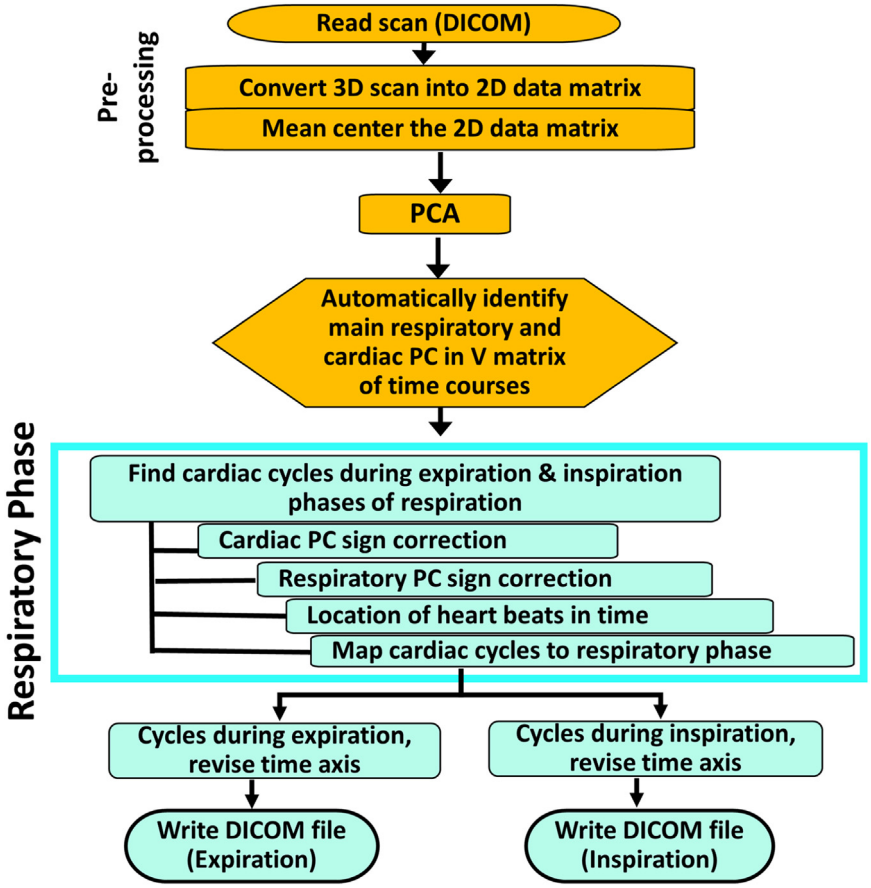


**Fig. 1.** Algorithm developed to group heartbeats by respiratory phase.

*2.3.2. Identification of cardiac cycles and their locations during respiration*

*2.3.2.1. Automatic identification of main respiratory and cardiac time courses.* Since ECG and respiratory navigation were not used during image acquisition, we obtained the time courses of the cardiac cycles and respiratory cycles retrospectively from PCA instead (Fig. 2). The software is configured to require an acquisition of at least 10 s to track more than one respiratory cycle and identify cardiac cycles both at end-inspiration and end-expiration. After resolving motional processes into PCs, the main time courses (PCs) of respiration and the heartbeat were identified automatically (Fig 2A) because the order of these key time courses varies among scans and subjects. To respiratory and cardiac time courses were identified by distinguishing respiratory rates from heart rates in the power spectra (Fourier transforms) of the oscillations of the PCs in real time (Fig. 2).

*2.3.2.2. Automatic recognition of cardiac cycles.* The cardiac time course (Fig 2) is affected by PCs being arbitrary in sign [42]. We defined systole as positive in sign based on the lesser brightness of the smaller volume of blood than during diastole (Fig S1). The starting point of each cycle is most consistently identifiable at end-systole, being narrower and more distinct than end-diastole (Fig 2A). A complete cardiac cycle spans from end-systole to end-systole and is determined by the algorithm seeking the cardiac time course crossing through an amplitude of zero (Fig. S1). For more precise placement of end-systole in time, the cardiac time course was fitted by cubic interpolation and smoothened with low-pass filtering. Smaller peaks near end-systole were rejected if within 0.4 s of a taller peak. For cardiac cycles that appeared longer than the mean length of a heartbeat by > 1.5 $\sigma$, a follow-up search lowered the threshold to find peaks near end-systole (taller than the weakest known end-systolic peak).

*2.3.3. DICOM files of cardiac cycles extract from expiration and inspiration*

The algorithm collected the heartbeats extracted from end-expiration in their original sequence (with jumps in time to the next respiration) into one DICOM file and the heartbeats extracted from end-inspiration in their original sequence into another DICOM file (Figs. S2 and S3). The resulting files were used for statistical analysis and assessment by cardiothoracic radiologists.

*2.3.4. Coding environments*

Algorithms to analyze PCs and their time courses were initially developed in MatLab version 2018b (MathWorks, Natick, MA). The algorithms were then ported to Python 3.7. A standalone version has been prepared for simple “two-click” operation under Windows.

*2.3.5. Operation of the new software for motion correction*

The step-by-step operation of the software is described at protocols.io: https://www.protocols.io/view/operation-of-software-for-motion-correction-of-car-36wgq72j5vk5/v1 . Please contact the corresponding author and Senior Technology Transfer Manager Adam Blumhagen at blumhagena@missouri.edu regarding licensing of the software.

*2.4. Evaluations*

*2.4.1. Statistical analysis*

2D correlation coefficients were calculated between corresponding voxel signal intensities of each frame at end-systole

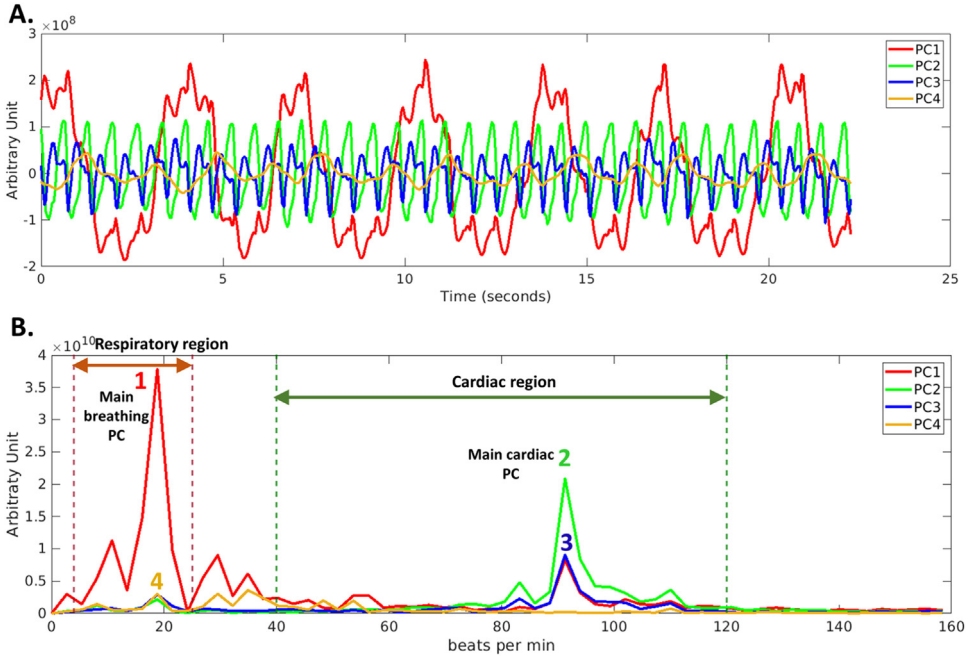


**Fig. 2.** Evaluation of time courses of major principal components for oscillations at respiratory and heart rates. (A) Plots of individual PC values vs. time of a three-chamber slice scan during free breathing. (B) Magnitude Fourier transforms of the time courses from panel A clarify the frequencies of the fluctuations.

with a single reference frame at end-systole from the beginning of the scan. For plots and paired-sample t-tests, the lowest correlation coefficient was selected from the set of correlation coefficients between frames. We also calculated the root-mean-squared deviation of the centers-of-brightness or centroids [43] within the heart. A paired samples *t*-test was performed for each evaluation metric before and after motion correction. Displacement field vectors were used to visualize local motions before and after motion correction. ImageJ was used to segment and measure areas [44] in the left ventricle. Bland-Altman plots [45] and Q-Q plots were used to assess comparability of methods.

*2.4.2. Expert scoring of cardiac imaging*

We presented images with and without retrospective motion correction to two expert cardiothoracic radiologists blinded to the post-processing. They evaluated the CMR quality in terms of blood-myocardial contrast, endocardial interface definition, and motion artifact. Each criterion was graded on a scale of 1 (insufficient) to 5 (excellent) (Table 2) on review of short axis slices.

## 3. Results

### *3.1. Resolution of cardiac cycles and phases*

The new algorithm identified the main principal components (PCs) at respiratory and cardiac contractile rates from power spectra of the PCs (Fig. 2). This achievement required optimization of the threshold at which the peak height at the respiratory rate was required to exceed the peak height at the heart rate, and vice versa (Fig. 2B). A ratio of 2.2 emerged from the optimization as adequate for the entire cohort of 20 subjects and their short axis and longitudinal scans, with heart rates up to 95/min and frame rates of 10 to 22/*sec*. The algorithm accurately corrected the sign of the *respiratory* PC in 93% of short axis and long axis scans, but interchanged labels on the expiratory and inspiratory subsets of cardiac cycles in 7% of scans. The algorithm corrected the sign of the *cardiac* PC accurately in 90% of short axis and long axis scans. The 10% of cardiac time courses without proper sign correction resulted in cardiac cycles being marked from end-diastole to end-diastole rather than end-systole to end-systole. The lengths of cardiac cycles from PCA of the CMR images agreed with the R-R lengths from ECG, but for potential skew at shorter heartbeats (Fig. S4).

### *3.2. Suppression of apparent breathing motion*

Suppression of respiratory motion in the background was validated by evaluating impact on movement of the heart (Figs. 3 and 4), reproducibility of frames from cardiac cycles (Fig. 5), and clinical assessments of the dynamic images (Fig. 7).

**Table 2**
Criteria used by cardiothoracic radiologists in scoring the images.

| Score | Blood-myocardial contrast (BMC) | Endocardial interface definition (EID) | Motion artifact (MA) |
|---|---|---|---|
| **1-Insufficient** | poor and nondiagnostic | poorly visible and images are nondiagnostic | Significant and images are nondiagnostic |
| **2- Poor** | poor but the images are diagnostic | significantly blurred | Significant and the images are nearly nondiagnostic |
| **3- Moderate** | Significant loss or variation throughout the cardiac cycle but the images are diagnostic | blurred, but images are diagnostic | visible but the images are diagnostic |
| **4- Good** | fairly uniform throughout the cardiac cycle and/or significantly bright blood pool | blurred during the cardiac cycle | Some present during the cardiac cycle but does not affect overall image quality |
| **5- Excellent** | uniform with little flashing; intensely bright blood pool | well defined in the bright blood pool | Images are nearly free of artifacts |

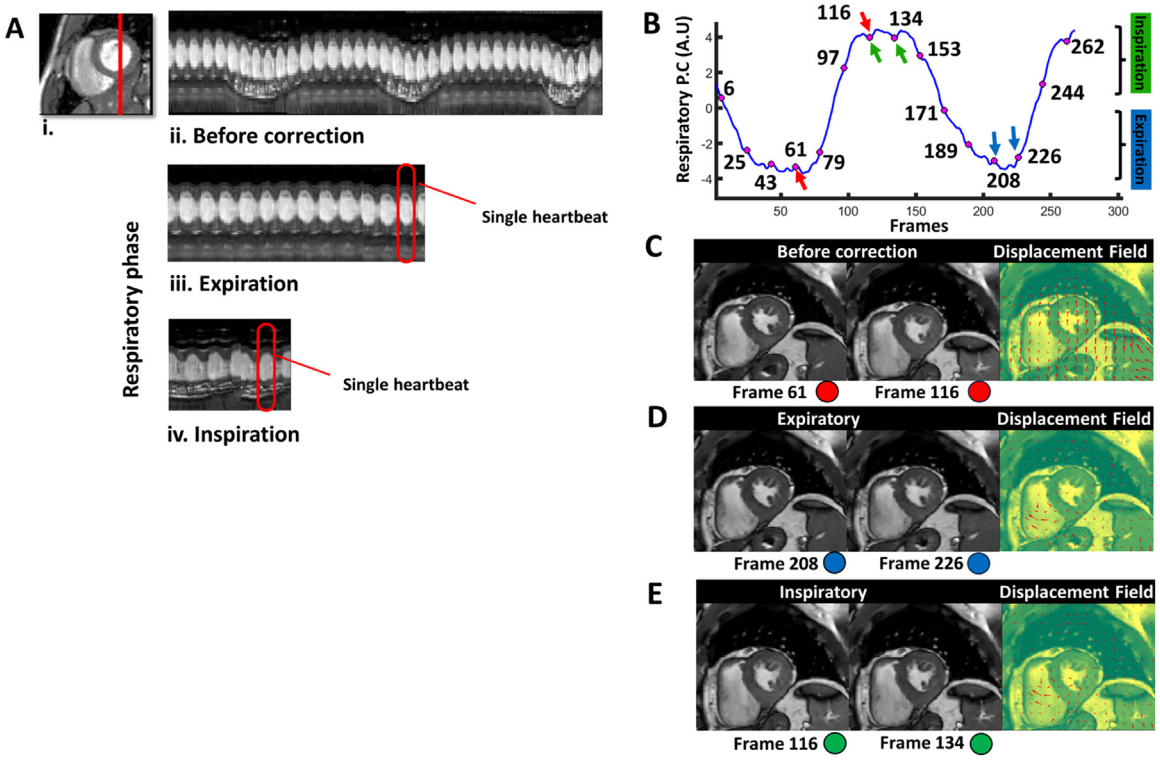


**Fig. 3.** Respiratory displacement of the heart in a short axis slice mitigated by respiratory phase. (A) A column of pixels (at the red line) is plotted from frames before (ii) and after grouping by respiratory phase (iii, iv). The red-highlighted region in (iii, iv) encloses a single heartbeat. (B) The respiratory PC is plotted over time. The endpoints of each heartbeat in time are indicated by magenta dots and frame numbers. Examples of respiratory displacement of the heart are shown before (C) and after grouping of heartbeats by respiratory phase (D,E). Displacement fields corresponding to the pairs of frames at matched systolic phases suggest displacement by respiration (C) or not (D,E). The position of the selected frames (C-E) in the respiratory time course (B) is color-coded using red to show respiratory change, blue for heartbeats at end-expiration, and green for heartbeats at inspiration.

### 3.2.1. *Evidence of less respiratory motion*

The decrease in apparent respiratory displacement of the heart upon separation of cardiac cycles from end-expiration or end-inspiration is illustrated in Fig. 3A. The suppression of apparent breathing

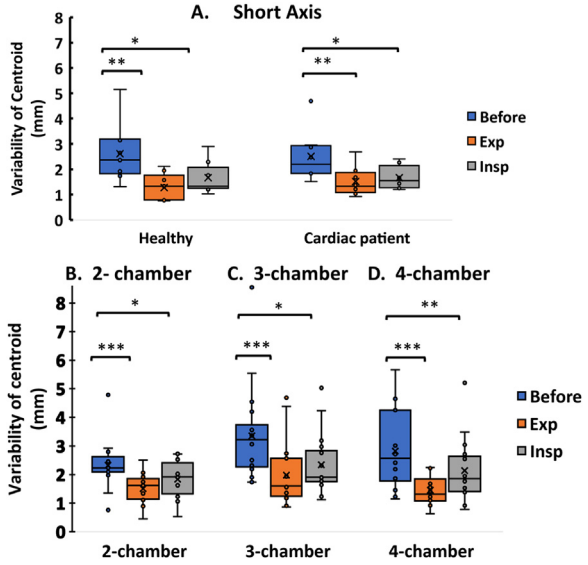


**Fig 4.** Variability of the centroid of real-time, dynamic CMRI scans, before and after grouping by respiratory phase. Results for short-axis views are shown in (A). Results for long-axis views are shown in the lower row for 2-chamber views (B), 3-chamber views (C), and 4-chamber views (D). The centroid is centered on the bright blood in the heart. Paired *t*-test results with $P \leq 0.05$, $P \leq 0.01$, or $P \leq 0.001$ are represented by *, **, or ***, respectively.

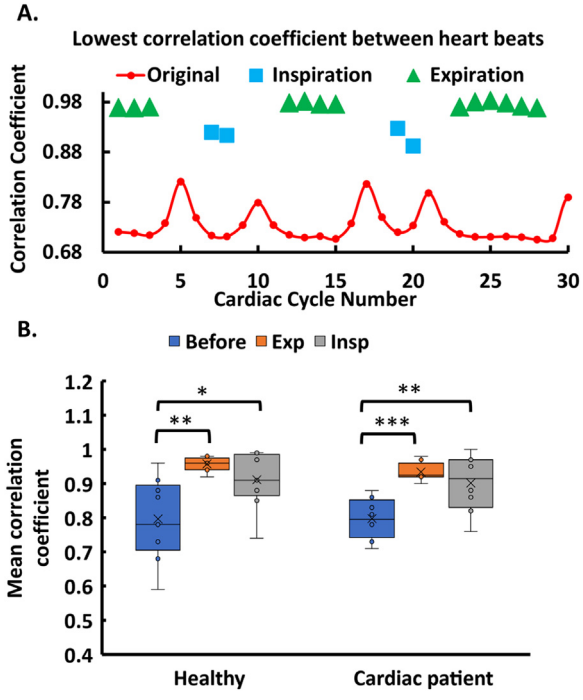


**Fig. 5.** Image consistency between heartbeats is improved by grouping the beats from end-expiration or end-inspiration. Correlation coefficients were calculated among the end-systolic frames of every heartbeat. Panel (A) shows one example of a short axis view. Panel (B) summarizes results for all SAX scans (for healthy controls and cardiac patients). Each point represents the average lowest correlation coefficient for a scan before and after grouping by respiratory phase. Each box plot shows the median as a horizontal line and the 25th and 75th percentiles as the edges of the box. Statistical significance with $P \leq 0.05$, $P \leq 0.01$, or $P \leq 0.001$ is indicated by *, **, or ***, respectively.

motion was even better at end-expiration than at end-inspiration. Respiratory displacement of the heart from end-expiration to end-inspiration is highlighted by the displacement field (Fig. 3B and C). The suppression of this respiratory displacement by grouping by respiratory phase is seen in Fig. 3D and C. Respiratory movement of the heart was monitored in all acquired scans using the center-of-brightness of the blood in the heart (Fig. 4). Inspiratory groups of heartbeats for both short axis and long axis views had less respiratory motion than the original scans ($P \leq 0.05$; Fig. 4). Expiratory groups of heart beats enjoyed more significant decreases of respiratory motions, both for short-axis views ($P \leq 0.01$) and long-axis views ($P \leq 0.001$; Fig. 4).

### 3.2.2. *Reproducibility of heartbeats*

The uniformity and reproducibility of the heartbeats was assessed using correlation coefficients between intensities of voxels of each frame at end-systole with a reference frame at end-systole. This was done both before and after motion correction. The smallest of those correlation coefficients are plotted in the example in Fig. 5A. This measure of the consistency of the heartbeats was compared by t-tests before and after correction of short axis view of the 19 subjects.

Motion-corrected images rendered the heartbeats clearly more consistent with one another (Fig. 5B). The improvements by respiratory grouping of heartbeats were statistically significant. The inspiratory groups of heartbeats improved the correlation coefficients with $P \leq 0.05$ for the healthy subjects and $P \leq 0.01$ for the subjects with histories of cardiac symptoms (Fig. 5B). The expiratory groups improved the correlation coefficients with $P \leq 0.01$ for the healthy subjects and $P \leq 0.001$ for the subjects with a history of cardiac symptoms. See Supplementary Videos S1, S2 (short axis view) and S3 (a long axis view) for examples of scans of subjects without and with segregation of cardiac cycles.

Ejection fractions estimated from areas [46] were compared for the first six cardiac cycles at end-expiration against cine CMR for ten subjects. The estimated ejection fractions at end-expiration encompassed those of cine CMR for seven of the ten subjects (Fig. 6). The ejection fractions estimated from end-expiration averaged almost 5% lower than those of cine, however (Fig. 6). The extremes at end-expiration ranged from 12% above to 18% below the reference ejection fraction estimated from cine CMR. The range in end-expiratory ejection fraction estimates averaged 7.7% per subject.

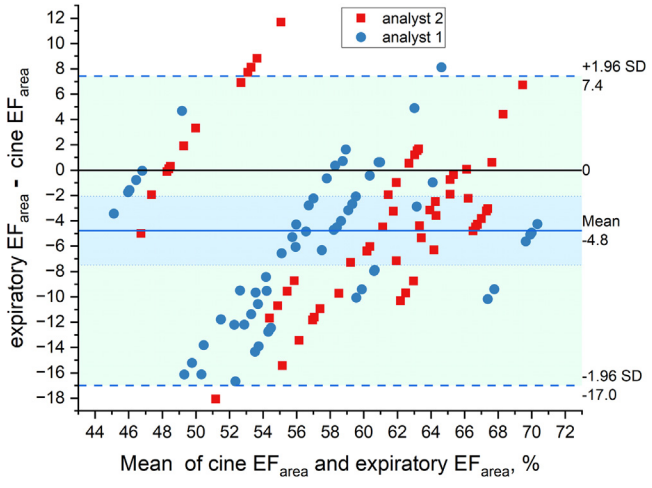


**Fig. 6.** Comparison of estimates of ejection fraction from real-time CMR at end-expiration with estimates from cine CMR. The first six cardiac cycles at end-expiration were compared with cine CMR for ten subjects (four healthy and six with a cardiac health history). Two analysts estimated ejection fractions from areas in single slices, $EF_{area}$, from manual segmentation. The Bland-Altman plot compares the estimates with six symbols for cardiac cycles at end-expiration (see the diagonal groups).

### 3.2.3. *Image evaluations by expert readers*

The qualities of the motion-corrected short-axis images from the cohort of volunteers were compared alongside the original images in blinded fashion by two expert cardiothoracic radiologists. The expert readers scored the image quality by criteria of blood-myocardial contrast, endocardial interface definition, and motion artifact (Table 2). The scores of image qualities of healthy subjects and heart patients before and after motion correction are shown in Fig. 7 by heatmaps representing the combined opinions of the two radiologists. Among the healthy subjects, the blinded scores across the three criteria were judged the same or better in 90% of the evaluations of images of cardiac cycles from expiration and in 60% of the evaluations of those from inspiration (Fig. 7A-F). Among the heart patients, the blinded scores were judged the same or better in 83% of images of cardiac cycles from expiration and 65% of those from inspiration (Fig 7G-L). However, the residual vertical displacement of the heart by inspiration increased the perceived motion artifact of cardiac cycles collected from inspiration in 56% of the healthy subjects and 36% of the heart patients (Fig. 7E, K). This perception could result from the large and varied vertical heart displacement in the inspiratory movies (Videos S1, S2). Nonetheless, the image quality was preserved or even enhanced in 86% of all images of cardiac cycles from expiration (Fig. 7).

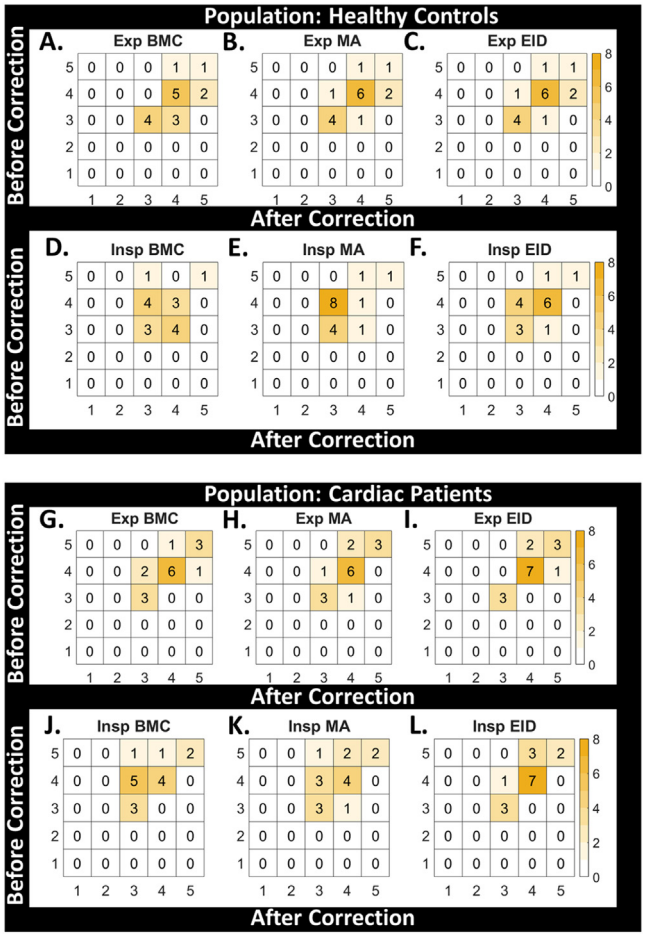


**Fig. 7.** Scores of image quality of short axis views of volunteers, before and after grouping by respiratory phase, by two expert radiologists blinded to the post-processing used. (A-F) Scores for the healthy volunteers are tabulated. (G-L) Scores for volunteers with cardiac symptoms. (A-C, G-I) These comparisons tally the scores before and after collecting beats from expiration. (D-F, J-L) These comparisons tally the scores before and after collecting beats from inspiration. (A,D,G,J) Blood-myocardial contrast (BMC). (B,E,H,K) Motion artifact (MA). (C,F,I,L) Endocardial interface definition (EID).

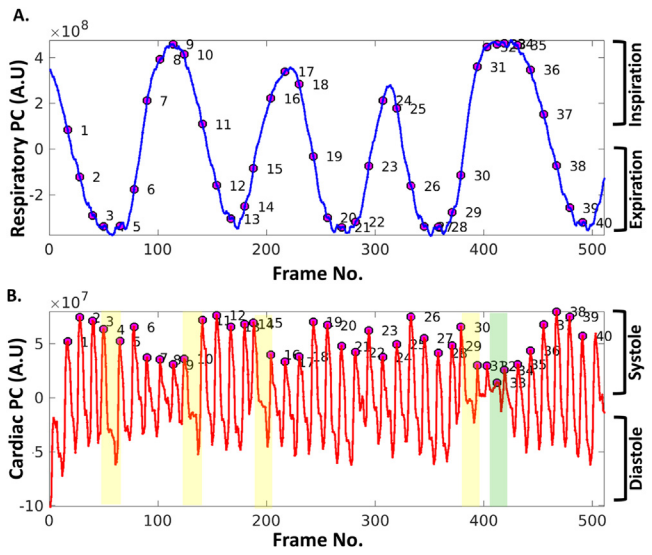


**Fig. 8.** Time courses of respiratory and cardiac PCs of a subject with an arrythmia. (A) Correct identification of the respiratory phases was confirmed by viewing the DICOM file of this 59-year-old male. (B) The cardiac cycles are divided end-systole to end-systole in the time course of the cardiac PC. Beats 4, 10, 15, and 30 were longer than usual (highlighted by yellow), and each followed a shorter-than-average beat. Beats 32 and 33 (highlighted by green) were shorter than usual.

### 3.3. Non-uniform respiratory and cardiac cycles

The performance of the grouping algorithm was scrutinized carefully on the challenging case of a subject with an arrythmia and non-uniform breathing. The algorithm worked in each essential step: The sign corrections of the time courses of the cardiac and respiratory PCs were accurate. Consequently, the software correctly assigned the end-inspiratory and end-expiratory phases (Videos S4 and S5) and the systolic and diastolic phases in the cardiac time courses (Fig. 8). The software correctly prepared the end-inspiratory and end-expiratory segments of the scans for all subjects with irregular breathing (subjects 15 – 18; results available at OSF repository). The software accurately divided the heartbeats from end-systole to end-systole despite the varying lengths of the cardiac cycles (Fig. 8B). Notably, the PCA-based division of the cardiac cycles identified heartbeats of unusual length, i.e., pairs in which a short beat was followed by a long beat (see yellow highlights in Fig. 8 and Video S6).

## 4. Discussion

### 4.1. Technical advances

We sought to enhance visualization of CMR scans collected during breathing in real-time without cardiac gating. Our objectives were to accommodate the breathing of the subject with less shifting of the heart position. Our new software decreased the apparent heart displacement by breathing, relative to other cardiac cycles of similar respiratory phase, especially at end-expiration. The heartbeats segregated by respiratory phase sometimes enhanced the apparent blood-myocardial contrast and endocardial edge delineation of some short axis scans acquired during breathing (Fig. 6). –These enhancements parallel the improved edge sharpness between myocardium and blood pool described for real-time CS acquisitions during free breathing [14,15]. When faced with irregular heart contractions and irregular breathing, this software utilizing PCA worked well in creating the inspiratory and expiratory portions of the original scan (Fig. 7, Videos S4 and S5). The algorithm exploits the capabilities of PCA of both *temporal* and spatial resolution [42,47,48]. PCA extraction of respiratory signals from dynamic medical images was validated against chest position [47,48]. Respiratory signals measured by hardware correlated highly with those extracted by PCA from CINE-CT or PET images [48] or from ungated CMR [47].

### 4.2. Anticipated relevance to patients

Real-time cardiac MRI, acquired rapidly by a variety of innovative methods, provides reliably high image quality [10]. By foregoing averaging, patients with an irregular heartbeat can be imaged, in principle. Other patients who are less compliant to averaged CMR might benefit by imaging during breathing. Such patients may include those suffering heart failure, dyspnea from COPD or asthma, or with a traumatic brain injury in the ICU. Mitigation of apparent respiratory motion in scans acquired during breathing, by this post-processing software or other methods, offer potential to relax expectations of regular heart rhythm, regular respiration, and breath holds. To the extent that real-time acquisitions might supplant breath-held parts of CMR exams, exams could become shorter [15,17] and more tolerable for non-compliant patients, while enhancing cost efficiency for clinics.

### 4.3. Limitations

The estimates of ejection fraction from end-expiratory cardiac cycles averaged almost 5% less than from cine CMR. The estimates of ejection fraction were based on area, however, rather than the standard of volume [46]. The software's post-processing time averaged 90 s per 3D DICOM file using a laptop with Intel i5 processor operating at 2.5 GHz under 64-bit Windows. The software can be deployed to a clinical workflow using a Docker image that acts after construction of the dynamic image. An earlier Siemens compressed sensing package acquired the real-time CMR scans of young adult volunteers at 22 frames/*sec*. However, software upgrades and subjects requiring larger field of view resulted in slower frame ratesand less spatial resolution. While the algorithm manages normal free breathing, it cannot correct for large through-plane motion in long axis views resulting from large displacements of the diaphragm from large inspirations. To compensate, subjects could be asked to breathe more shallowly during imaging. The study was limited to small numbers of volunteers.

## Conclusions

We enhanced the visualization of free-breathing, dynamic cardiac MRI images of small numbers of healthy and symptomatic subjects. This was achieved by segregating cardiac cycles from end-expiration and end-inspiration phases of respiration by post-processing. The technical strategy is novel and distinct from methods reliant upon image registration. The post-processing strategy is vendor-neutral and neutral to the type of real-time image acquisition. The software could merit trial with a broader range of real-time image acquisitions. The combination of real-time acquisitions with this post-processing software offers the potential to facilitate CMR scanning of patients non-compliant to cine protocols. This includes patients too frail for multiple breath holds and patients with arrhythmias unsuitable for averaging. The improved visualization of free-running CMR by respiratory phase fosters possibilities of visualizing the variability of cardiac cycles with respiratory phase and arrhythmias. Despite residual motion artifacts during deep breaths in, inspiratory groups of cardiac cycles might reveal effects of inspiration upon cardiac behavior. The image quality of the cardiac cycles from expiration is superior, and attractive for wider evaluation.

## Data availability

The data are fully available without restriction. The results generated for each human subject (anonymized) are available at the OSF repository under doi:10.17605/OSF.IO/4UNBE at https://osf.io/4unbe/. The data available include real-time cardiac MRI scans before and after motion correction by respiratory phase (.avi movie format). Plots of the time courses of respiration, heart contraction, and improvement in correlation coefficients are also available for each subject.

Academic licensing of the software developed can be requested by contacting the corresponding author and the Office of Technology Advancement (email: blumhagena@missouri.edu). Commercial licenses are also available by contacting the Senior Technology Transfer Manager at blumhagena@missouri.edu, as well as the corresponding author.

## CRediT authorship contribution statement

**Ummul Afia Shammi:** Investigation, Methodology, Software, Formal analysis, Validation, Visualization, Data curation, Writing – original draft. **Zhijian Luan:** Software. **Jia Xu:** Methodology, Software. **Aws Hamid:** Validation. **Lucia Flors:** Validation. **Joanne Cassani:** Resources, Writing – review & editing. **Talissa A. Altes:** Supervision, Resources, Funding acquisition. **Robert P. Thomen:** Methodology, Validation, Supervision, Funding acquisition, Writing – review & editing. **Steven R. Van Doren:** Conceptualization, Methodology, Data curation, Writing – original draft, Supervision, Project administration, Funding acquisition.

## Declaration of Competing Interest

The authors declare the following financial interests/personal relationships which may be considered as potential competing interests:

Steven R. Van Doren reports support was provided by the University of Missouri Coulter Biomedical Accelerator. Steven Van Doren, Ummul Afia Shammi, Robert Thomen, Zhijian Luan, Jia Xu, Talissa Altes have provisional patent application #U.S. Provisional Patent Application Serial No. 63/337,464 'REAL-TIME CARDIAC MAGNETIC RESONANCE (MR) BY RESPIRATORY PHASE' to Steven Van Doren, Ummul Afia Shammi, Robert Thomen, Zhijian Luan, Jia Xu, Talissa Altes.

## CRediT authorship contribution statement

**Ummul Afia Shammi:** Investigation, Methodology, Software, Formal analysis, Validation, Visualization, Data curation, Writing – original draft. **Zhijian Luan:** Software. **Jia Xu:** Methodology, Software. **Aws Hamid:** Validation. **Lucia Flors:** Validation. **Joanne Cassani:** Resources, Writing – review & editing. **Talissa A. Altes:** Supervision, Resources, Funding acquisition. **Robert P. Thomen:** Methodology, Validation, Supervision, Funding acquisition, Writing – review & editing. **Steven R. Van Doren:** Conceptualization, Methodology, Data curation, Writing – original draft, Supervision, Project administration, Funding acquisition.

## Supplementary materials

Supplementary material associated with this article can be found, in the online version, at doi:10.1016/j.redii.2023.100035.

## References

[1] Constantine G, Shan K, Flamm SD, Sivananthan MU. Role of MRI in clinical cardiology. Lancet 2004;363:2162–71. doi: 10.1016/S0140-6736(04)16509-4.

[2] Kramer CM, Barkhausen J, Bucciarelli-Ducci C, Flamm SD, Kim RJ, Nagel E. Standardized cardiovascular magnetic resonance imaging (CMR) protocols: 2020 update. J Cardiovasc Magn Reson 2020;22:17. doi: 10.1186/s12968-020-00607-1.

[3] Barkhausen J, Goyen M, Rühm SG, Eggebrecht H, Debatin JF, Ladd ME. Assessment of ventricular function with single breath-hold real-time steady-state free precession cine MR imaging. Am J Roentgenol 2002;178:731–5. doi: 10.2214/ajr.178.3.1780731.

[4] Gulati M, Levy PD, Mukherjee D, Amsterdam E, Bhatt DL, Birtcher KK, Blankstein R, Boyd J, Bullock-Palmer RP, Conejo T, Diercks DB, Gentile F, Greenwood JP, Hess EP, Hollenberg SM, Jaber WA, Jneid H, Joglar JA, Morrow DA, O'Connor RE, Ross MA, Shaw LJ. 2021 AHA/ACC/ASE/CHEST/SAEM/SCCT/SCMR guideline for the evaluation and diagnosis of chest pain. J Am Coll Cardiol 2021;78:e187–285. doi: 10.1016/j.jacc.2021.07.053.

[5] Zhang S, Joseph AA, Voit D, Schaetz S, Merboldt K-D, Unterberg-Buchwald C, Hennemuth A, Lotz J, Frahm J. Real-time magnetic resonance imaging of cardiac function and flow—Recent progress, Quant. Imaging Med Surg 2014;4:313–29 http://qims.amegroups.com/article/view/4050.

[6] Yang PC, Kerr AB, Liu AC, Liang DH, Hardy C, Meyer CH, Macovski A, Pauly JM, Hu BS. New real-time interactive cardiac magnetic resonance imaging system complements echocardiography. J Am Coll Cardiol 1998;32:2049–56. doi: 10.1016/S0735-1097(98)00462-8.

[7] Barnett LA, Prior JA, Kadam UT, Jordan KP. Chest pain and shortness of breath in cardiovascular disease: a prospective cohort study in UK primary care. BMJ Open 2017;7. doi: 10.1136/bmjopen-2017-015857.

[8] Strauss-Blasche G, Moser M, Voica M, McLeod D, Klammer N, Marktl W. Relative timing of inspiration and expiration affects respiratory sinus arrhythmia. Clin Exp Pharmacol Physiol 2000;27:601–6. doi: 10.1046/j.1440-1681.2000.03306.x.

[9] Agelink MW, Malessa R, Baumann B, Majewski T, Akila F, Zeit T, Ziegler D. Standardized tests of heart rate variability: normal ranges obtained from 309 healthy humans, and effects of age, gender, and heart rate. Clin Auton Res 2001;11:99–108. doi: 10.1007/BF02322053.

[10] Nayak KS, Lim Y, Campbell-Washburn AE, Steeden J. Real-time magnetic resonance imaging. J Magn Reson Imaging 2022;55:81–99. doi: 10.1002/jmri.27411.

[11] Voit D, Zhang S, Unterberg-Buchwald C, Sohns JM, Lotz J, Frahm J. Real-time cardiovascular magnetic resonance at 1.5 T using balanced SSFP and 40ms resolution. J Cardiovasc Magn Reson 2013;15:79. doi: 10.1186/1532-429X-15-79.

[12] Haji-Valizadeh H, Rahsepar AA, Collins JD, Bassett E, Isakova T, Block T, et al. Validation of highly accelerated real-time cardiac cine MRI with radial k-space sampling and compressed sensing in patients at 1.5T and 3T. Magn Reson Med 2018;79:2745–51. doi: 10.1002/mrm.26918.

[13] Hauptmann A, Arridge S, Lucka F, Muthurangu V, Steeden JA. Real-time cardiovascular MR with spatio-temporal artifact suppression using deep learning—proof of concept in congenital heart disease. Magn Reson Med 2019;81:1143–56. doi: 10.1002/mrm.27480.

[14] Longère B, Allard P-E, Gkizas CV, Coisne A, Hennicaux J, Simeone A, Schmidt M, Forman C, Toupin S, Montaigne D, Pontana F. Compressed sensing real-time cine reduces CMR arrhythmia-related artifacts. J Clin Med 2021:10. doi: 10.3390/jcm10153274.

[15] Longère B, Abassebay N, Gkizas C, Hennicaux J, Simeone A, Rodriguez Musso A, Carpentier P, Coisne A, Pang J, Schmidt M, Toupin S, Montaigne D, Pontana F. A new compressed sensing cine cardiac MRI sequence with free-breathing real-time acquisition and fully automated motion-correction: a comprehensive evaluation. Diagn Interv Imaging 2023. doi: 10.1016/j.diii.2023.06.005.

[16] Sudarski S, Henzler T, Haubenreisser H, Dösch C, Zenge MO, Schmidt M, Nadar MS, Borggrefe M, Schoenberg SO, Papavassiliu T. Free-breathing sparse sampling cine MR imaging with iterative reconstruction for the assessment of left ventricular function and mass at 3.0 T. Radiology 2017;282:74–83. doi: 10.1148/radiol.2016151002.

[17] Vermersch M, Longère B, Coisne A, Schmidt M, Forman C, Monnet A, Pagniez J, Silvestri V, Simeone A, Cheasty E, Montaigne D, Pontana F. Compressed sensing real-time cine imaging for assessment of ventricular function, volumes and mass in clinical practice. Eur Radiol 2020;30:609–19. doi: 10.1007/s00330-019-06341-2.

[18] Lin L, Li Y, Wang J, Cao L, Liu Y, Pang J, An J, Jin Z, Wang Y. Free-breathing cardiac cine MRI with compressed sensing real-time imaging and retrospective motion correction: clinical feasibility and validation. Eur Radiol 2023;33:2289–300. doi: 10.1007/s00330-022-09210-7.

[19] Piekarski E, Chitiboi T, Ramb R, Feng L, Axel L. Use of self-gated radial cardiovascular magnetic resonance to detect and classify arrhythmias (atrial fibrillation and premature ventricular contraction). J Cardiovasc Magn Reson 2016;18:83. doi: 10.1186/s12968-016-0306-6.

[20] Unterberg-Buchwald C, Fasshauer M, Sohns JM, Staab W, Schuster A, Voit D, Kowallick JT, Steinmetz M, Frahm J, Lotz J. Real time cardiac MRI and its clinical usefulness in arrhythmias and wall motion abnormalities. J Cardiovasc Magn Reson 2014;16:P34. doi: 10.1186/1532-429X-16-S1-P34.

[21] Allen BD, Carr ML, Markl M, Zenge MO, Schmidt M, Nadar MS, Spottiswoode B, Collins JD, Carr JC. Accelerated real-time cardiac MRI using iterative sparse SENSE reconstruction: comparing performance in patients with sinus rhythm and atrial fibrillation. Eur Radiol 2018;28:3088–96. doi: 10.1007/s00330-017-5283-0.

[22] Ahmad R, Hu HH, Krishnamurthy R, Krishnamurthy R. Reducing sedation for pediatric body MRI using accelerated and abbreviated imaging protocols. Pediatr Radiol 2018;48:37–49. doi: 10.1007/s00247-017-3987-6.

[23] Steeden JA, Kowalik GT, Tann O, Hughes M, Mortensen KH, Muthurangu V. Real-time assessment of right and left ventricular volumes and function in children using high spatiotemporal resolution spiral bSSFP with compressed sensing. J Cardiovasc Magn Reson 2018;20:79. doi: 10.1186/s12968-018-0500-9.

[24] Longère B, Pagniez J, Coisne A, Farah H, Schmidt M, Forman C, Silvestri V, Simeone A, Gkizas CV, Hennicaux J, Cheasty E, Toupin S, Montaigne D, Pontana F. Right ventricular volume and function assessment in congenital heart disease using CMR compressed-sensing real-time cine imaging. J Clin Med 2021;10. doi: 10.3390/jcm10091930.
[25] Jakob PM, Griswold MA, Edelman RR, Manning WJ, Sodickson DK. Accelerated cardiac imaging using the SMASH technique. J Cardiovasc Magn Reson 1999;1:153–7. doi: 10.3109/10976649909080844.
[26] Kühl HP, Spuentrup E, Wall A, Franke A, Schröder J, Heussen N, Hanrath P, Günther RW, Buecker A. Assessment of myocardial function with interactive non–breath-hold real-time MR imaging: comparison with echocardiography and breath-hold cine MR imaging. Radiology 2004;231:198–207. doi: 10.1148/radiol.2311021237.
[27] Bustin A, Fuin N, Botnar RM, Prieto C. From compressed-sensing to artificial intelligence-based cardiac MRI reconstruction. Front Cardiovasc Med 2020;7. doi: 10.3389/fcvm.2020.00017.
[28] Usman M, Atkinson D, Odille F, Kolbitsch C, Vaillant G, Schaeffter T, Batchelor PG, Prieto C. Motion corrected compressed sensing for free-breathing dynamic cardiac MRI. Magn Reson Med 2013;70:504–16. doi: 10.1002/mrm.24463.
[29] Baron CA, Dwork N, Pauly JM, Nishimura DG. Rapid compressed sensing reconstruction of 3D non-Cartesian MRI. Magn Reson Med 2018;79:2685–92. doi: 10.1002/mrm.26928.
[30] Bilal M, Shah JA, Qureshi IM, Kadir K. Respiratory motion correction for compressively sampled free breathing cardiac MRI using smooth l(1)-norm approximation. Int J Biomed Imaging 2018;2018:7803067. doi: 10.1155/2018/7803067.
[31] Feng L, Grimm R, Block KT, Chandarana H, Kim S, Xu J, Axel L, Sodickson DK, Otazo R. Golden-angle radial sparse parallel MRI: combination of compressed sensing, parallel imaging, and golden-angle radial sampling for fast and flexible dynamic volumetric MRI. Magn Reson Med 2014;72:707–17. doi: 10.1002/mrm.24980.
[32] Lustig M, Donoho D, Pauly JM, Sparse MRI. The application of compressed sensing for rapid MR imaging. Magn Reson Med 2007;58:1182–95. doi: 10.1002/mrm.21391.
[33] Zhou R, Yang Y, Mathew RC, Mugler JP, Weller DS, Kramer CM, Ahmed AH, Jacob M, Salerno M. Free-breathing cine imaging with motion-corrected reconstruction at 3T using SPiral Acquisition with Respiratory correction and Cardiac Self-gating (SPARCS). Magn Reson Med 2019;82:706–20. doi: 10.1002/mrm.27763.
[34] Wang J, Zhou R, Wang X, Awad M, Salerno M. Free-breathing high-resolution spiral real-time cardiac cine imaging at 1.5 T with deep learning-based spiral image reconstruction (DESIRE). In: ISMRM 30th Annual Scientific Session, ISMRM; 2022.
[35] Kellman P, Chefd'hotel C, Lorenz CH, Mancini C, Arai AE, McVeigh ER. Fully automatic, retrospective enhancement of real-time acquired cardiac cine MR images using image-based navigators and respiratory motion-corrected averaging. Magn Reson Med 2008;59:771–8. doi: 10.1002/mrm.21509.
[36] Crum WR, Hartkens T, Hill DLG. Non-rigid image registration: theory and practice. Br J Radiol 2004;77:S140–53. doi: 10.1259/bjr/25329214.
[37] Makela T, Clarysse P, Sipila O, Pauna N, Pham QC, Katila T, Magnin IE. A review of cardiac image registration methods. IEEE Trans Med Imaging 2002;21:1011–21. doi: 10.1109/TMI.2002.804441.
[38] Xue H, Kellman P, LaRocca G, Arai AE, Hansen MS. High spatial and temporal resolution retrospective cine cardiovascular magnetic resonance from shortened free breathing real-time acquisitions. J Cardiovasc Magn Reson 2013;15:102. doi: 10.1186/1532-429X-15-102.
[39] Han Z, Thornton-Wells TA, Dykens EM, Gore JC, Dawant BM. Effect of nonrigid registration algorithms on deformation-based morphometry: a comparative study with control and Williams syndrome subjects. Magn Reson Imaging 2012;30:774–88. doi: 10.1016/j.mri.2012.02.005.
[40] Bieri O, Scheffler K. Fundamentals of balanced steady state free precession MRI. J Magn Reson Imaging 2013;38:2–11. doi: 10.1002/jmri.24163.
[41] Schär M, Kozerke S, Fischer SE, Boesiger P. Cardiac SSFP imaging at 3 Tesla. Magn Reson Med 2004;51:799–806. doi: 10.1002/mrm.20024.
[42] Xu J, Van Doren SR. Tracking equilibrium and nonequilibrium shifts in data with TREND. Biophys J 2017;112:224–33. doi: 10.1016/J.BPJ.2016.12.018.
[43] McManus IC, Stöver K, Kim D. Arnheim's Gestalt theory of visual balance: examining the compositional structure of art photographs and abstract images. Iperception 2011;2:615–47. doi: 10.1068/i0445aap.
[44] Schneider CA, Rasband WS, Eliceiri KW. NIH Image to ImageJ: 25 years of image analysis. Nat Methods 2012;9:671–5. doi: 10.1038/nmeth.2089.
[45] Martin Bland J, Altman D. Statistical methods for assessing agreement between two methods of clinical measurement. Lancet 1986;327:307–10. doi: 10.1016/S0140-6736(86)90837-8.
[46] Wisneski JA, Pfeil CN, Wyse DG, Mitchell R, Rahimtoola SH, Gertz EW. Left ventricular ejection fraction calculated from volumes and areas: underestimation by area method. Circulation 1981;63:149–51. doi: 10.1161/01.CIR.63.1.149.
[47] Novillo F, Van Eyndhoven S, Moeyersons J, Bogaert J, Claessen G, La Gerche A, Van Huffel S, Claus P. Unsupervised respiratory signal extraction from ungated cardiac magnetic resonance imaging at rest and during exercise. Phys Med Biol 2019;64:065001. doi: 10.1088/1361-6560/ab02cd.
[48] Thielemans K, Rathore S, Engbrant F, Razifar P. Device-less gating for PET/CT using PCA. 2011 IEEE nuclear science symposium conference record; 2011. p. 3904–10. doi: 10.1109/NSSMIC.2011.6153742.